ELSEVIER

Sensitivity of biogenic secondary organic aerosols to future climate change at regional scales: An online coupled simulation

Xiaoyan Jiang [a], Zong-Liang Yang [a,*], Hong Liao [b], Christine Wiedinmyer [c]

[a] Department of Geological Sciences, The John A. and Katherine G. Jackson School of Geosciences, 1 University Station #C1100, The University of Texas at Austin, Austin, TX 78712-0254, USA
[b] State Key Laboratory of Atmospheric Boundary Layer Physics and Atmospheric Chemistry (LAPC), Institute of Atmosphere Physics, Chinese Academy of Sciences, Beijing 100029, China
[c] The National Center for Atmospheric Research, Boulder, CO 80307-3000, USA

ARTICLE INFO

ABSTRACT

Biogenic emissions and secondary organic aerosols (SOA) are strongly dependent on climatic conditions. To understand the SOA levels and their sensitivity to future climate change in the United States (U.S.), we present a modeling work with the consideration of SOA formation from the oxidation of biogenic emissions with atmospheric oxidants (e.g., OH, O_3, and NO_3). The model simulation for the present-day climate is evaluated against satellite and ground-based aerosol measurements. Although the model underestimates aerosol concentrations over the northwestern U.S. due to the lack of fire emissions in the model simulations, overall, the SOA results agree well with previous studies. Comparing with the available measurements of organic carbon (OC) concentrations, we found that the amount of SOA in OC is significant, with the ratio ranging from 0.1 to 0.5/0.6. The enhanced modeling system driven by global climate model output was also applied for two three-year one-month simulations (July, 2001–2003 and 2051–2053) to examine the sensitivity of SOA to future climate change. Under the future two emissions scenarios (A1B and A2), future temperature changes are predicted to increase everywhere in the U.S., but with different degrees of increase in different regions. As a result of climate change in the future, biogenic emissions are predicted to increase everywhere, with the largest increase (∼20%) found in the southeastern and northwestern U.S. under the A1B scenario. Changes in SOA are not identical with those in biogenic emissions. Under the A1B scenario, the biggest increase in SOA is found over Texas, with isoprene emissions being the major contributor to SOA formation. The range of change varies from 5% over the southeast region to 26% over Texas. The changes in either biogenic emissions or SOA under the two climate scenarios are different due to the differences in climatic conditions. Our results also suggest that future SOA concentrations are also influenced by several other factors such as the partitioning coefficients, the atmospheric oxidative capability, primary organic carbon aerosols and anthropogenic emissions.

1. Introduction

Secondary organic aerosols (SOA) that are formed in the atmosphere through oxidation with precursor volatile organic compounds (VOC) exert, along with other aerosol components, an important impact on radiation and the hydrological cycle (e.g., Chung and Seinfeld, 2002; Kanakidou et al., 2005; Barth et al., 2005; Hoyle et al., 2009). However, impacts of SOA on climate relative to other aerosols remain highly uncertain due to the lack of direct measurements on large scales and less understanding of their formation. SOA can be formed from the oxidation of

anthropogenic VOCs and biogenic VOCs (BVOCs). On a large scale, BVOCs are estimated to be the predominant source (e.g., Andersson-Skold and Simpson, 2001; Tsigaridis and Kanakidou, 2003; Kanakidou et al., 2005).

Thanks to recent progress achieved from laboratory experiments (e.g., Griffin et al., 1999; Kroll et al., 2006; Offenberg et al., 2006; Kroll and Seinfeld, 2008), and ambient measurements (e.g., Claeys et al., 2004; Pun and Seigneur, 2008), our understanding of SOA formation chemistry has recently improved. With knowledge obtained from laboratory experiments, SOA formation has been parameterized in models (e.g., Chung and Seinfeld, 2002; Donahue et al., 2006; Jimenez et al., 2009). Traditional SOA models (e.g., Chung and Seinfeld, 2002; Tsigaridis and Kanakidou, 2003; Heald et al., 2008) use a two-product absorptive partitioning scheme (Odum et al.,

* Corresponding author. Tel.: +1 512 471 3824; fax: +1 512 471 9425.
E-mail address: liang@jsg.utexas.edu (Z.-L. Yang).

1997), which assumes that only two semi-volatile products are formed from the oxidation of a parent hydrocarbon by an oxidant. This approach has some limitations. It neglects the contributions from VOC oxidation products of high and intermediate volatility. It does not include second-generation chemistry to SOA formation, the importance of which was illustrated by Ng et al. (2006). Several recent studies (e.g., Robinson et al., 2007; Donahue et al., 2006, 2009) have made efforts to improve SOA parameterizations. For instance, Donahue et al. (2006) presented a new framework for organic aerosol modeling. The volatility basis set in their study spans a larger range of atmospheric conditions than the two-product model does, and conveniently accounts for partitioning, dilution, and chemical aging of organic vapors. Robinson et al. (2007) proposed an organic aerosol model scheme based on lumping species into volatility bins of a basis set, and their results show a good agreement with ambient measurements. However, emission inventories for volatility basis set approach do not exist. Thus, in this study, we use the two-product approach. SOA formation has also been included in regional (Griffin et al., 2002; Zhang et al., 2008) and global (e.g., Tsigaridis and Kanakidou, 2003; Lack et al., 2004; Tsigaridis et al., 2005; Henze and Seinfeld, 2006; Liao et al., 2007; Heald et al., 2008) models to study SOA burden. At global scales, Tsigaridis et al. (2005) studied the variability of SOA distributions and budget to natural climate variability by incorporating a SOA scheme in a global 3-dimensional chemistry transport model. Liao et al. (2007) included a SOA scheme in a global chemistry model and evaluated model performance with the available ground-based aerosol products over the U.S. Their results reveal that SOA contributes 5–38% of fine particles with diameter less than 2.5 μm ($PM_{2.5}$) in different regions of the U. S.

Climate affects SOA concentrations in the atmosphere via temperature, precipitation and changing the oxidative capacity of the atmosphere. In the meantime, changes in temperature also influence the amount of precursor emissions of SOA, in particular, biogenic emissions. The interest to study the effects of potential future climate change on air quality including ozone and aerosols has risen significantly during the past few years (e.g., Tagaris et al., 2007; Jiang et al., 2008; Jacob and Winner, 2009). Several studies (Liao et al., 2006; Tsigaridis and Kanakidou, 2007; Heald et al., 2008) have studied the sensitivity of SOA to future climate change, and they found that increased biogenic emissions due to an increase in temperature account for most of the changes in SOA. The largest future increase in SOA from 2000 to 2100 is predicted by Tsigaridis and Kanakidou (2007). And they also found that in 2100, SOA burden will exceed that of sulfate, suggesting the importance of SOA in the atmosphere. Heald et al. (2008) studied the sensitivity of SOA to changes in future climate, anthropogenic emissions and land use using a global climate model. They found that climate change alone does not change the global mean SOA, while the rising of biogenic emissions and anthropogenic emissions can result in an increase of 36% in SOA in 2100. Although their studies examined different factors in controlling SOA concentrations, the regional details are not well represented. On regional scales, Zhang et al. (2008) examined the sensitivity of air quality to potential regional climate change in the United States (U.S.) using down-scaled climate output. They found that models underestimate by at least 20% of the responses of organic aerosols to future climate change if SOA formation is not included. These studies suggest that understanding the response of SOA change to climate change is important not only for air quality studies, but also for climatic effects.

In the current study, we mainly focus on biogenic SOA from BVOCs. It should be noted that anthropogenic VOCs contribute to SOA formation much more than previously believed (e.g., Heald et al., 2008; Farina et al., 2010). An evaluation of the contribution of anthropogenic VOCs to SOA formation over the U.S. will be the subject of future studies. In addition, SOA from BVOC precursors and/or their oxidation products can also form via aqueous phase processing in cloud droplets and atmospheric particles (Carlton et al., 2006; Volkamer et al., 2009; El Haddad et al., 2009) or gas-phase hydrolysis (Axson et al., 2010). The omission of these processes may result in underestimation of SOA in our results. As our understanding on the aqueous phase aerosol improves, this needs to be considered in SOA formation. The objectives of this study are twofold: to investigate detailed SOA levels over the contiguous U.S. using a coupled land–atmosphere–chemistry model; and to understand how SOA burden will respond to future climate change under different emissions scenarios on a regional scale. We first include a SOA model in an existing coupled model to evaluate the model performance. We then employ this modified model to examine the sensitivity of SOA to different future climate change scenarios. We begin in Section 2 with a description of the coupled model and SOA model. In Section 3, we evaluate the model results against available satellite and ground-based measurements. Finally, we discuss the effects of future climate change on biogenic SOA formation.

2. Model description

2.1. WRF/Chem model

The chemistry version of the physically-based Weather Research and Forecasting (WRF) model (Skamarock et al., 2005)— referred as the WRF/Chem model (Grell et al., 2005) thereafter—is used in this study. In the WRF/Chem, both the meteorological and the air quality components are mutually consistent in that they employ the same transport scheme (mass and scalar preserving), grid (horizontal and vertical components), physics schemes for subgrid-scale transport, land surface models, and timestep. That means all transport of chemical species is done online. The dynamic core we use in this study is the mass coordinate version of the model, called Advanced Research WRF (ARW). The gas-phase chemistry used in this study is based on the CBM-Z mechanism

Table 1
Hydrocarbon classes of reactive biogenic emissions.

Hydrocarbon class	Composition
I	α-pinene, β-pinene, sabinene, Δ^3-carene, terpenoid ketones
II	Limonene
III	α-terpinene, γ-terpinene, terpinolene
IV	myrcene, terpenoid, alcohols, ocimene
V	isoprene

Table 2
Description of oxidation products.

Lumped products	Description
SOG1	lumped 9 gas-phase products from oxidation of hydrocarbon class I, II, and III
SOG2	lumped 3 gas-phase products from oxidation of hydrocarbon class IV
SOG3	lumped 2 gas-phase products from oxidation of hydrocarbon class V
SOA1	lumped 9 aerosol phase products from oxidation of hydrocarbon class I, II, and III
SOA2	lumped 3 aerosol phase products from oxidation of hydrocarbon class IV
SOA3	lumped 2 aerosol phase products from oxidation of hydrocarbon class V

(Zaveri and Peters, 1999). This scheme uses 67 prognostic species and 164 reactions in a lumped structure approach according to their internal bond types. It is similar to the widely used carbon bond mechanism (CBM-IV), but is extended for use on different spatial and temporal scales. Fast-J photolytic reactions are used within CBM-Z (Wild et al., 2000; Barnard et al., 2004). The model for simulating aerosol interactions and chemistry (MOSAIC) (Zaveri et al., 2008) is used in this work to simulate aerosols. MOSAIC treats several major aerosol species including sulfate, methanesulfonate, nitrate, chloride, carbonate, ammonium, sodium, calcium, black carbon, primary organic mass and liquid water. Gas-phase species are allowed to partition into the particle phase. The size distributions of aerosols are represented using a sectional approach based on dry particle diameters. In this study, we use four discrete size bines. Dry deposition of trace gases from the atmosphere to the surface is calculated by multiplying concentrations in the lowest model by the spatially and temporally varying deposition velocity. The deposition velocity is proportional to the sum of three characteristic resistances (aerodynamic resistance, sublayer resistance, surface resistance). The surface resistance parameterization used in the dry deposition scheme is developed by Wesley (1989). Dry deposition of aerosol number and mass is based on Binkowski and Shankar (1995) and is calculated using the wet size of particles. Simplified wet deposition by convective parameterization with scavenging factor of 0.6 for aerosols is used in the current study. Wet deposition considering in cloud and below-cloud wet removal will be used in future studies when the aerosol-cloud feedback is treated in the model.

2.2. Secondary organic aerosol model

The version of WRF/Chem used in this study is version 2.2, which does not include a SOA module with the selected gas-phase and aerosol schemes, thus we follow the idea of the two-product model approach to describe SOA formation in the WRF/Chem based on the method used in Chung and Seinfeld (2002) and Liao et al. (2007). As this is the simplest way to represent SOA formation, it could lead to some uncertainties in the modeling results. In addition, heterogeneous and aqueous phase reactions forming SOA are not included in the current model since the level of understanding is still low. Although it is important to accurately represent all factors in the model, all model results are subject to uncertainty. Rate constants and aerosol yield parameters determined from laboratory chamber results (Seinfeld and Pankow, 2003) are used in the SOA model. A complete implementation of SOA formation from monoterpenes and other reactive VOCs (ORVOCs) in a global model was described by Chung and Seinfeld (2002). Isoprene has recently been recognized to contribute to a significant amount of SOA in nature (e.g., Claeys et al., 2004; Zhang et al., 2007; Carlton et al., 2009; Karl et al., 2009). Some studies have started to include isoprene as a source of SOA in global and regional models (Henze and Seinfeld, 2006; Liao et al., 2007; Zhang et al., 2007, 2008; Heald et al., 2008). Following their approaches, we implement a SOA module in the WRF/Chem with the consideration of oxidation of monoterpenes, isoprene and ORVOC emissions. We include oxidation of monoterpenes and ORVOC emissions with OH, O_3 and NO_3, whereas considering oxidation of isoprene emissions with only OH. Formation of SOA from photooxidation of isoprene emissions in this work is based on the work of Henze and Seinfeld (2006), in which they presented results of chamber experiments about reaction of isoprene emissions with OH at low NO_x condition (Kroll et al., 2006). Though reaction with O_3 or NO_3 may also lead to SOA formation, the magnitudes of these sources are assumed to be minor (Calvert et al., 2000).

As in the work of Chung and Seinfeld (2002), monoterpenes and ORVOCs are divided into five hydrocarbon classes according to

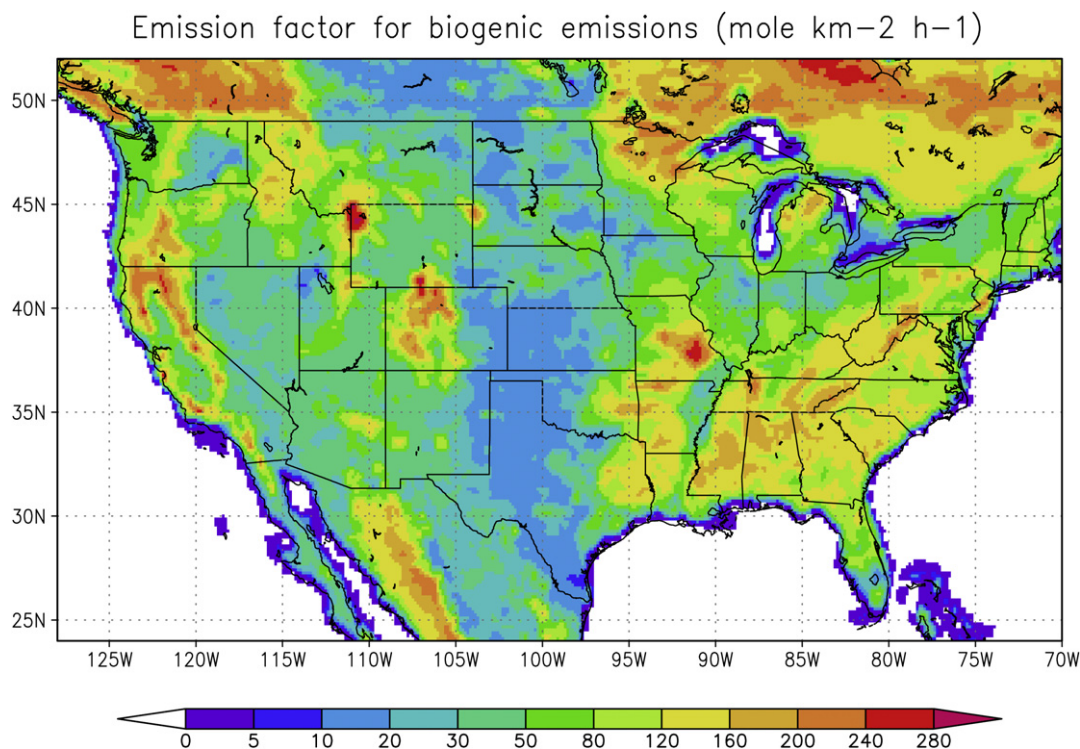**Fig. 1.** BVOC emissions under standard climatic condition of light, temperature, soil moisture, humidity and leaf conditions, including a leaf area index of 5, a canopy with 92% mature leaves, a solar angle of 60°, a photosynthetic photon flux density transmission of 0.6, air temperature of 303 K, humidity at 14 g kg^{-1}, and soil moisture at 0.3 m^3 m^{-3}. (mole km^{-2} h^{-1}).
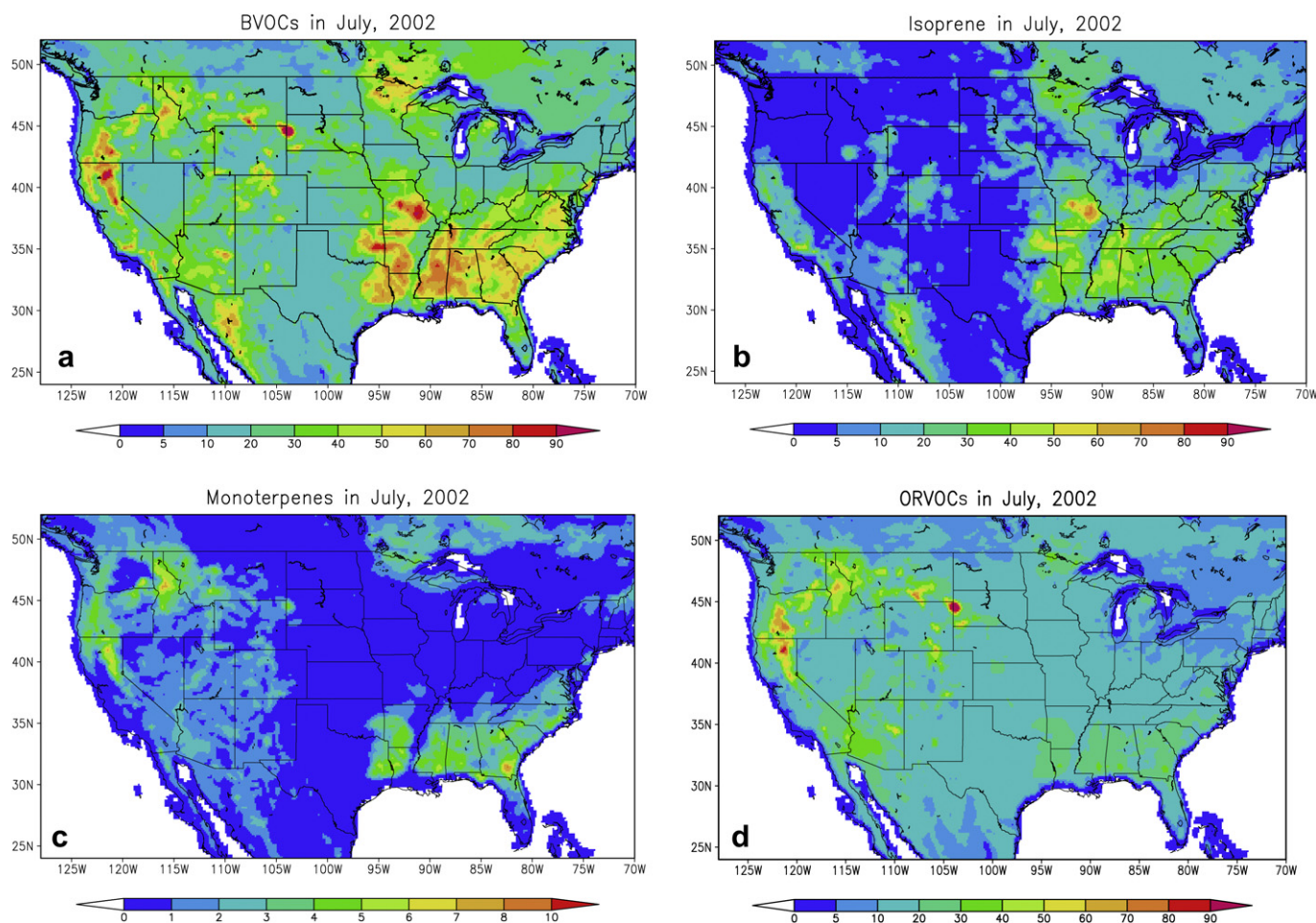
Fig. 2. Model calculated BVOCs (a), Isoprene (b), Monoterpenes (c) and ORVOCs (d) in July, 2002 (mole km^{-2} h^{-1}).

the values of their experimentally measured aerosol yield parameters (Griffin et al., 1999). In this work, biogenic emissions are calculated with the Biogenic Emissions Inventory System, version 3 (BEIS3) (Vukovich and Pierce, 2002) in the WRF/Chem. Species calculated in the BEIS3 model are different from those used in Chung and Seinfeld (2002). Thus, following their approach, we categorized monoterpenes and ORVOCs into four reactive biogenic hydrocarbon groups excluding sesquiterpenes due to the lack of emission estimates in the current model (BEIS3) (Table 1). Short-lived sesquiterpenes have been shown to produce a substantial amount of SOA, and the magnitude of formed SOA can be as large as that from monoterpenes (Sakulyanontvittaya et al., 2008), thus we need to be aware that the simulated SOA concentrations in the present study may be underestimated. Isoprene is included as hydrocarbon class V. The fraction of monoterpenes is from Table 4 of Griffin et al. (1999). For each of the first four reactive hydrocarbon classes, there are three oxidation products, two for combined O_3 and OH oxidation and one for NO_3 oxidation. Reaction of isoprene with oxidants generates two oxidation products. The mass-based stoichiometric coefficients (α_i) for all reactions are presented in Table 3. The partition coefficients K_i corresponding to α_i are also listed in Table 3. All products are semi-volatile, and they partition between the gas and aerosol phases. Thus, there are a total of 28 oxidation products. In the model, we use SOG1, SOG2, and SOG3 to represent lumped gas-phase products from oxidation of hydrocarbon classes I, II and III, from hydrocarbon class IV and from hydrocarbon class V

respectively (Table 2). SOA1, SOA2 and SOA3 are lumped aerosol phase products from oxidation of these five hydrocarbon classes (Table 2).

All products are semi-volatile and can partition between gas and aerosol phases. The partitioning of these products between gas phase (G_i) and aerosol (A_i) is represented by the partitioning theory (Pankow, 1994),

$$G_i = A_i/(K_iM_0) \tag{1}$$

in which K_i represents partitioning coefficient and M_o represents pre-existing absorptive organic matter. In the partitioning process, the effect of temperature is considered according to the temperature dependence of saturation concentrations derived from Clausius–Clapeyron equation (Baum, 1998):

$$K_i\left(T_{ref}\right) = K_i(T)\left(T_{ref}/T\right)\exp\left(\Delta H_{vap}/R\left(1/T_{ref} - 1/T\right)\right) \tag{2}$$

where T_{ref} is set at 295 K for isoprene and 310 K for others; R is ideal gas constant; T is temperature. The heat of vaporization for organic compounds is from the CRC Handbook of Chemistry and Physics (Lide, 2001), $\Delta H_{vap} = 42$ KJ mol^{-1} is used for all compounds. Dry deposition of SOA follows the method used for gas-phase species, in which the surface resistance is defined by Wesley (1989). Simplified wet deposition by convective parameterization with scavenging factor of 0.6 (Chin et al., 2000) is used for SOA in the current study.

2.3. Anthropogenic and biogenic emissions

The anthropogenic emissions inventory of gas and aerosol species is the U.S. EPA's 1999 National Emissions Inventory (NEI-99, version 3) released in 2003 (http://www.epa.gov/air/data/neidb.html). The emissions are derived by temporal allocation factors specific to each source classification code provided by the EPA. They are representative of a typical summer day. This inventory has been successfully used in the WRF/Chem simulations (Jiang et al., 2008). A more detailed description of this anthropogenic emissions inventory can be found in Jiang et al. (2008). Biogenic emissions are very sensitive to changes in temperature and radiation. Emission rates of biogenic compounds at standard temperature and light conditions have been assigned to the model grid on the basis of BEIS3 and the Biogenic Emissions Landuse Database, version 3 (BELD3), which provides distributions of 230 vegetation classes at 1-km resolution over North America (Kinnee et al., 1997). Fig. 1 shows the BVOCs emissions under standard climatic condition of light, temperature, soil moisture, humidity and leaf conditions, including a leaf area index of 5, a canopy with 92% mature leaves, a solar angle of 60°, a photosynthetic photon flux density transmission of 0.6, air temperature of 303 K, humidity at 14 g kg^{-1}, and soil moisture at 0.3 m^3 m^{-3}. Then, biogenic emissions in all simulations are calculated online using the temperature and light-dependence algorithms from the BEIS3. Emissions from biomass burning, sea-salt and dusts are not considered in the current study.

3. Experiment design

The first part of this study is to investigate the SOA levels over the U.S. for the present-day climate using the modified WRF/Chem model with the inclusion of SOA formation. The modeling domain covers the entire contiguous U.S. on a 32-km horizontal grid. There are a total of 28 vertical model layers, with finer vertical resolution in the lower troposphere to allow the model to simulate boundary−layer processes more realistically. The highest emissions of BVOCs from the vegetation occur between June and August (Guenther et al., 1995), thus production of SOA from the oxidation of biogenic emissions will be most relevant during that period. To thoroughly understand the SOA levels in the U.S., multi-year simulations would be preferred. However, to run multi-year simulations with this fully coupled land−atmosphere−chemistry model demands a huge amount of computing time. Under this circumstance, we carefully selected one month, July 2002 to represent summer season to examine the model performance in terms of simulating BVOCs and SOA. The initial and lateral boundary meteorological conditions required by the WRF/Chem are from the NCEP's North American Regional Reanalysis (NARR) data set, which has a domain covering our configured computational area (Mesinger et al., 2006). As aforementioned, anthropogenic emissions are from the NEI-99 and biogenic emissions are calculated online.
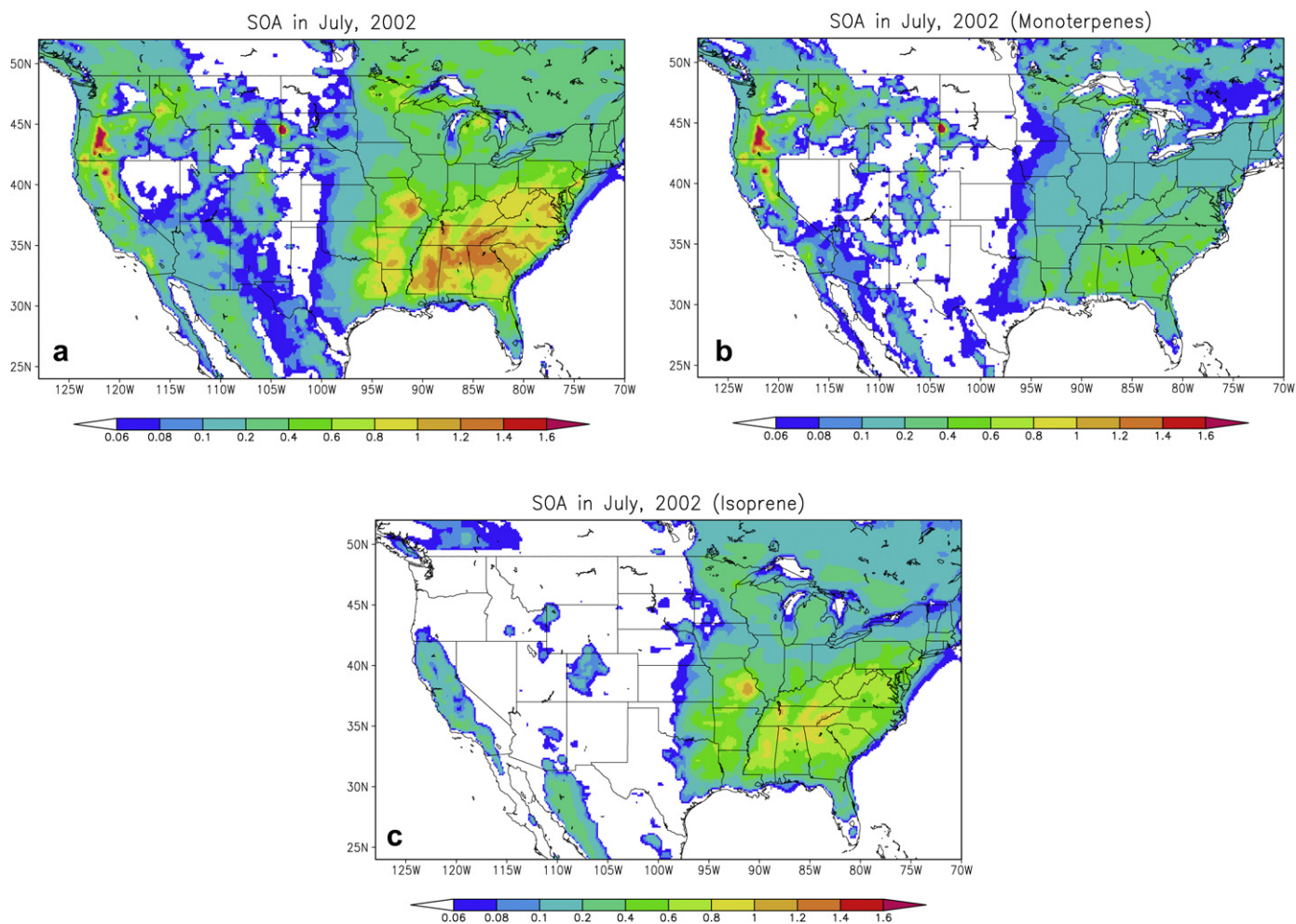

Fig. 3. Model simulated concentrations of total SOA (a), SOA from monoterpenes (b) and SOA from isoprene (c) in July, 2002 (μg m^{-3}).

The second objective of this study is to understand the effects of potential future climate change on SOA concentrations on regional scales. A series of experiments using global climate model projections as initial and lateral meteorological boundary conditions are conducted. The output of global climate model—Community Climate System Model 3.0 (CCSM3)—is used to provide different future climate scenarios. The CCSM3 has been used for the 4th Assessment Report of the Intergovernmental Panel on Climate Change (IPCC) (Collins et al., 2006), and the horizontal resolution is T85 ($\sim$1.41°). Readers are referred to Meehl et al. (2006) for a full analysis of the CCSM3 future climate simulations. The greenhouse gas concentrations during the CCSM3 simulation period used in this study follow the IPCC Special Report on Emission Scenarios (SRES) A1B and A2 (IPCC, 2001). The emissions scenarios, built on storylines that link emissions to different driving forces, are described in detail in Nakicenovic et al. (2000). The A1B scenario is associated with increasing trace gases and aerosol concentrations from 2001 until 2050. It is a mid-line scenario for carbon dioxide output and economic growth. As an alternative, the A2 scenario, which is based on a world that is regionally organized economically, technological change, is fragmented, and population growth is high, is also selected to test the sensitivity of SOA formation to different climate scenarios. The CCSM3 output has been successfully applied to WRF/Chem simulations on a relatively high spatial resolution (Jiang et al., 2008). Most previous studies about the impacts of future climate change on regional air quality or aerosol concentrations rely on downscaled regional climate model output

(e.g., Hogrefe et al., 2004; Zhang et al., 2008; Avise et al., 2009). In this study, the WRF/Chem is a fully coupled regional model including online atmosphere and land surface models, thus, the regional downscaling of climate and SOA simulation are performed simultaneously with the WRF/Chem. For this part of study, we also selected July to represent summer situation. In previous studies of the impacts of climate change on O_3 (e.g., Hogrefe et al., 2004; Liao et al., 2006) and aerosols (e.g., Tagaris et al., 2007; Heald et al., 2008; Zhang et al., 2008), authors used either a few (e.g., two) summer seasons or a few (e.g., one or two years) years to study the impacts. Thereby, we designed our experiments for three consecutive Julys to represent the present and future scenarios respectively. We simulated a current period (2001—2003, denoted as "current") and a future period (2051—2053, denoted as "future"). In future work, with increasingly available computational resource, multi-year runs would be the optimal way to statistically assess the changes. The differences between the future-year and current-year simulations are used to assess the impacts of climate change on SOA formation. The anthropogenic emissions for the present-day simulations are also applied for the future-year simulations to avoid any impacts from changes in anthropogenic emissions on our results. Biogenic emissions for the future-years are simulated online with the BEIS3 scheme.

To minimize the effect of initial conditions on model results, the initial 2-day period (June 29 and 30) of each simulation was considered as a spin-up period to establish the initial conditions for several atmospheric concentrations of different emission species. In
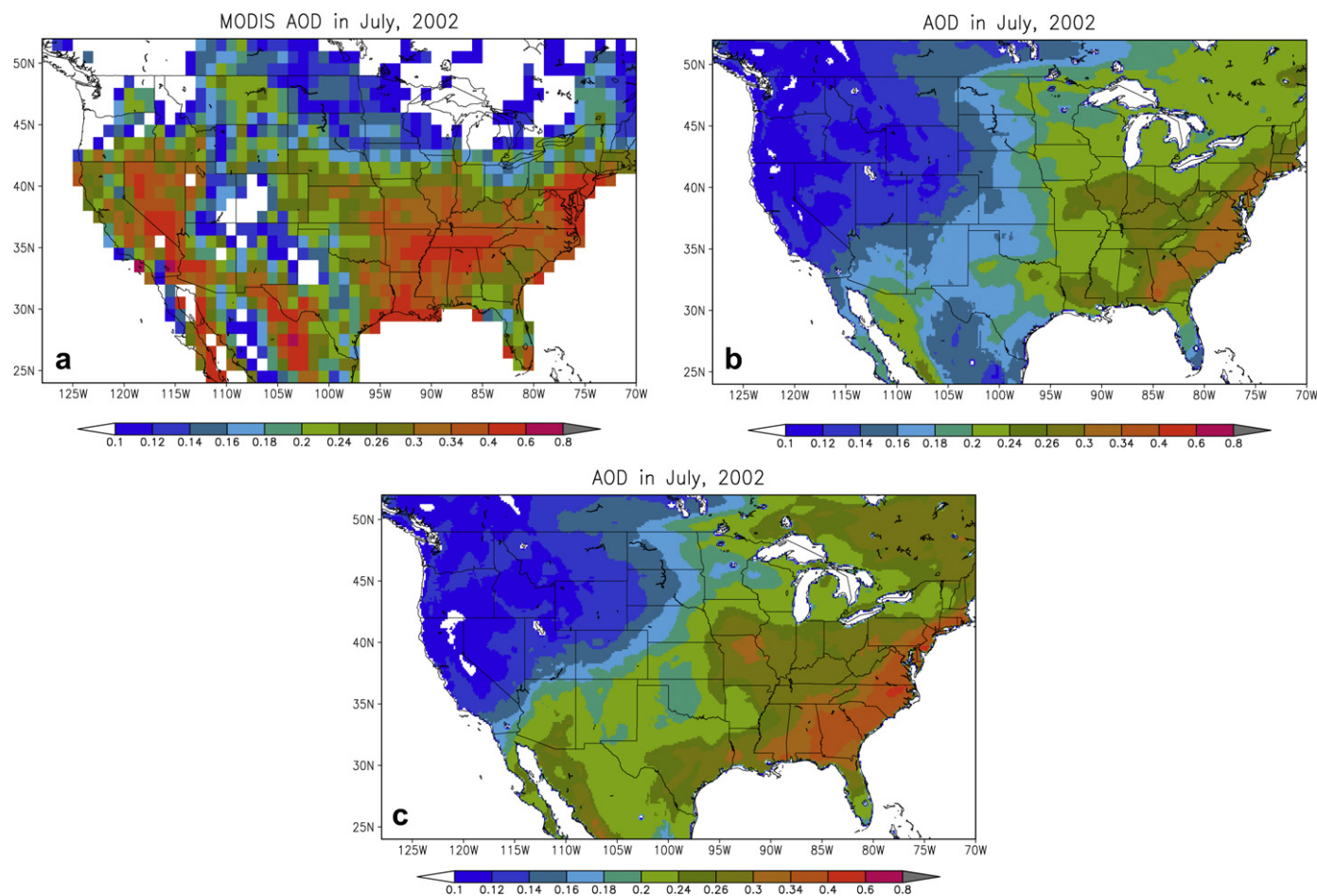

Fig. 4. Aerosols optical depth (AOD): (a) MODIS derived monthly level-2 product, (b) Model simulated with SOA formation, and (c) Model simulated with SOA included.

all simulations, we used the same set of gas-phase chemistry (CMB-Z) and aerosol scheme (MOSAIC). Other parameterizations used in all simulations include the Lin et al.'s microphysics scheme (Lin et al., 1983), the Kain-Fritsch Cumulus Parameterization scheme (Kain and Fritsch, 1990), the Yonsei University Planetary Boundary Layer (PBL) scheme (Hong and Pan, 1996), the Simple Cloud Interactive Radiation scheme (Dudhia, 1989), the Rapid Radiative Transfer Model Longwave Radiation scheme (Mlawer et al., 1997) and the Noah LSM.

4. Present-day simulation of biogenic SOA

In this section, we first present the simulated distributions of biogenic emissions and SOA. Then we compare model results with available satellite and ground-based aerosol measurements to evaluate model performance.

4.1. Regional distributions of biogenic emissions and SOA

Fig. 2 shows the spatial plots of the online calculated total biogenic emissions, isoprene, monoterpenes and ORVOCs in July, 2002. Simulated spatial pattern of total biogenic emissions in July agrees with the patterns simulated by several previous studies (e.g., Guenther et al., 1995; Levis et al., 2003). High emissions occur where there's a significant amount of vegetation, such as the

southeastern and northwestern U.S. The simulated spatial patterns of isoprene and monoterpenes are slightly different, which is attributed to the different emission capacities of different types of vegetation. Example trees emitting isoprene are deciduous trees (Kesselmeier and Staudt, 1999) such as oak trees, which are more dominant in the southern U.S. including Texas. Coniferous trees such as pines, cedars and firs, which exist over the northwestern U.S., emit a significant amount of monoterpenes. Overall, the model shows reasonable skill in simulating the spatial patterns of biogenic emissions over the U.S.

Fig. 3a shows the spatial pattern of mean surface concentrations of SOA in July, 2002. The concentrations of SOA range up to 1.6 $\mu g \ m^{-3}$, and the maximum values are found over the regions where there are high concentrations of BVOC emissions (the northwestern and southeastern U.S.). Over the northwestern U.S., a majority of SOA comes from the oxidation of monoterpenes (Fig. 3b), while over the southeastern U.S., the contribution of isoprene is dominant (Fig. 3c). The results suggest the importance of including isoprene emissions in SOA formation. The simulated SOA concentrations of 0.4–1.6 $\mu g \ m^{-3}$ are predicted over the two major regions, and SOA levels predicted over other regions (e.g., northeast) are around 0.2–0.8 $\mu g \ m^{-3}$. Comparing with other studies (e.g., Liao et al., 2007), the simulated SOA levels are reasonable, but more regional details are simulated in the present study.
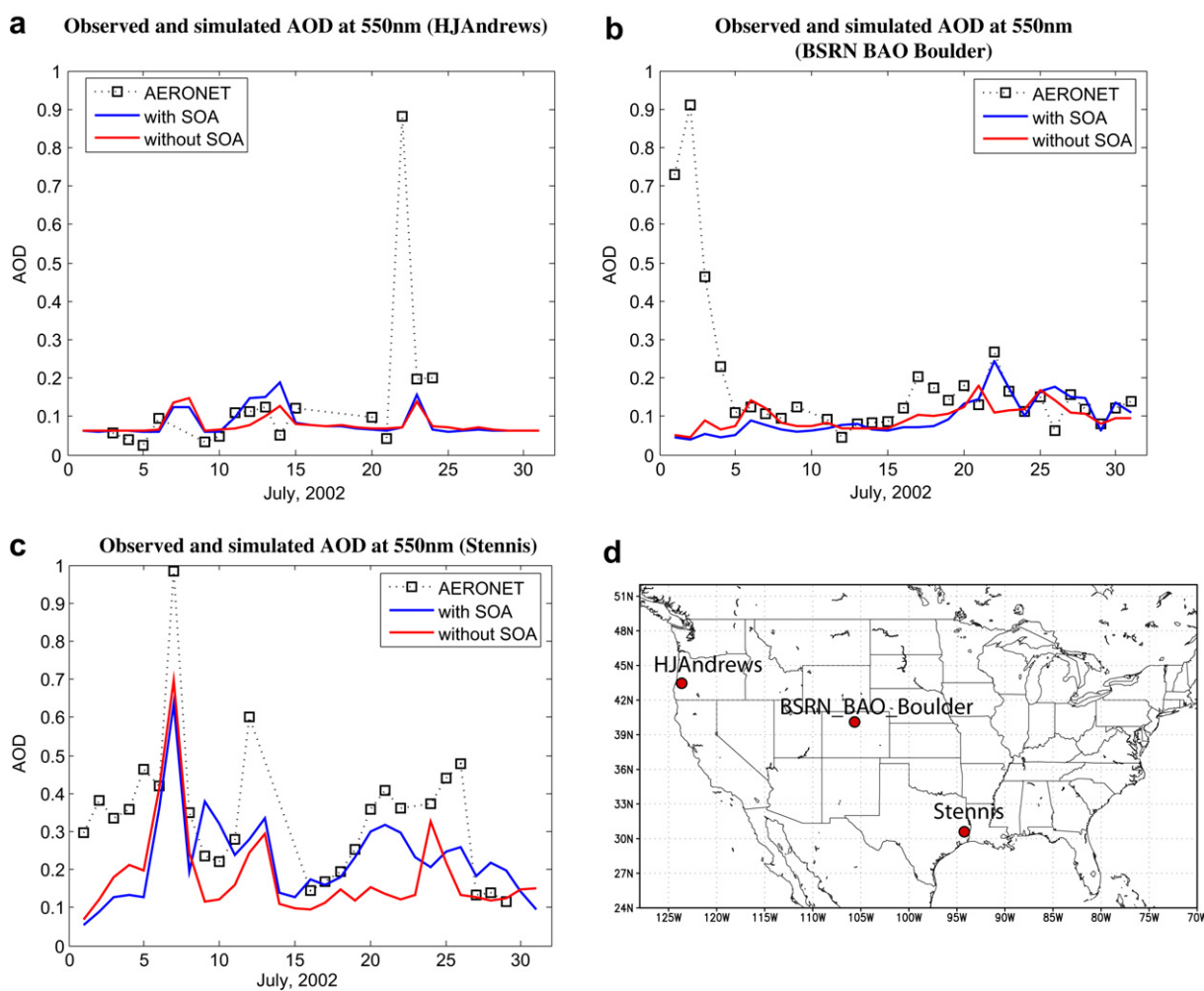

Fig. 5. AERONET measured and model simulated AOD at three sites (a) HJAndrews, (b) BSRN_BAO_Boulder and (c) Stennis. (d) is a map showing the three locations.
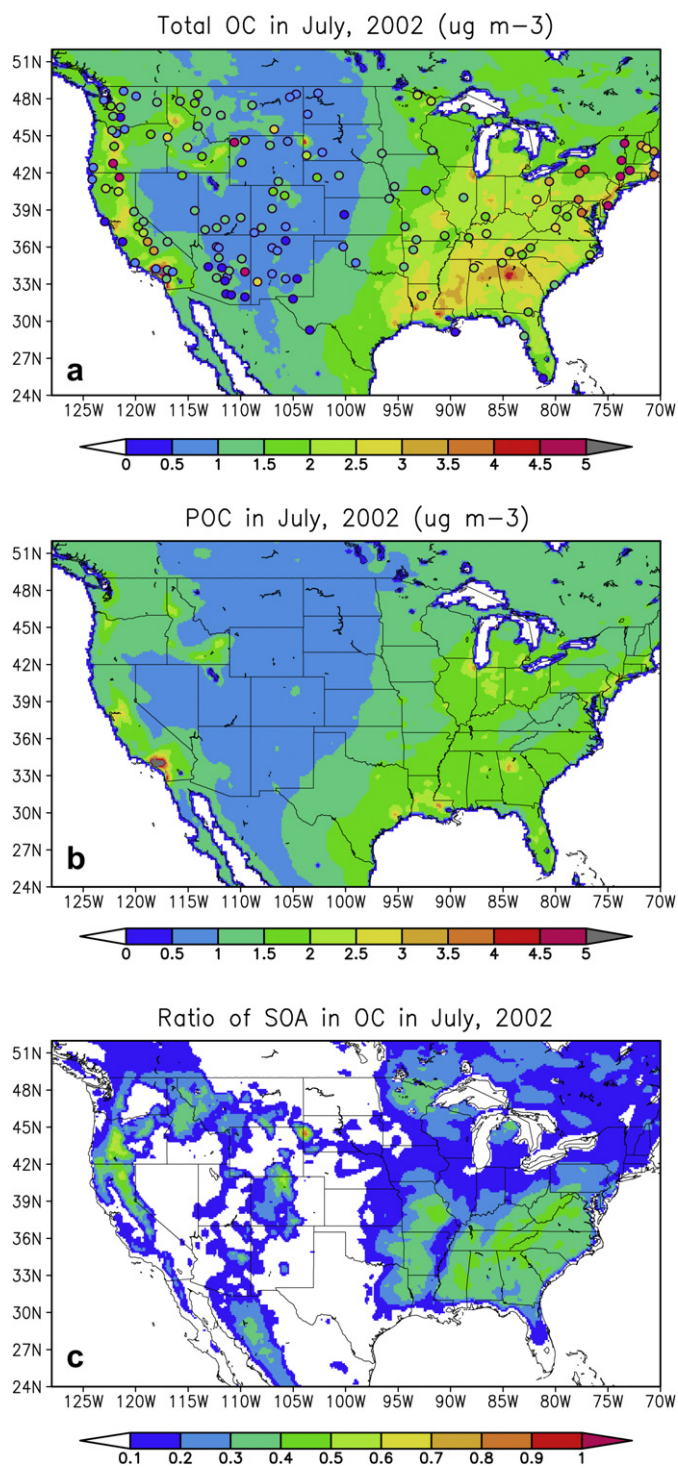
Total OC in July, 2002 (ug m−3)

POC in July, 2002 (ug m−3)

Ratio of SOA in OC in July, 2002

Fig. 6. (a) Model simulated and measured (at IMPROVED sites) monthly mean surface layer OC (Primary OC (POC) + SOA) concentrations (μg m^{-3}), (b) POC and (c) ratio of SOA in OC in July, 2002.

4.2. Comparison with observations

Model performance is the key to understanding SOA levels over the U.S. Measurements of organic aerosols under ambient atmospheric conditions generally do not distinguish between primary and secondary sources. One common way is to use other relevant aerosol products to evaluate model performance. In this subsection, spatial and temporal distributions of model simulated aerosol

optical property and concentrations are compared with MODIS (Moderate Resolution Imaging Spectroradiometer) − derived aerosol optical depth (AOD), AOD from Aerosol Robotic Network (AERONET) and organic carbon aerosol concentrations from the ground-based measurement network of the Interagency Monitoring of Protected Visual Environments (IMPROVE) (http://vista.cira.colostate.edu/improve/).

To compare with the available AOD measurements, we calculated AOD using Mie theory in the WRF/Chem. The details regarding the treatment of aerosol optical properties can be found in Fast et al. (2006). The aerosol optical properties in the WRF/Chem are calculated at four wavelengths, 300, 400, 600, and 1000 nm. For the MODIS AOD product, monthly MOD04 level-2 product at 550 nm wavelength with a spatial resolution of 1-degree is used for model evaluation on a monthly basis. The AERONET measurements are site-specific with wavelengths up to eight wavelengths (1640, 1020, 870, 675, 500, 440, 380 and 340 nm). Level 2.0 (quality-assured) data are used in this study (Smirnov et al., 2000). MODIS AOD is directly retrieved at 550 nm, whereas model calculated AOD and AERONET AOD are not at 550 nm. As the three AOD datasets are at different wavelengths, the comparisons are made at 550 nm wavelength. We used Angstrom exponent relation (http://disc.sci.gsfc.nasa.gov/data-holdings/PIP/aerosol_angstrom_exponent.shtml) to derive AOD at 550 nm for both model output and AERONET data based on AOD at the near wavelengths. For instance, for the AERONET data, the Angstrom exponent between wavelengths 440 and 675 nm was used to derive AERONET AOD at 550 nm using the following equation:

$$\tau_2 = \tau_1/\exp[-\alpha\ln(\lambda_1/\lambda_2)]; \tag{3}$$

where τ_2 is the AOD at 550 nm, τ_1 is the AOD at 500 nm, α is the Angstrom exponent between 440 and 675 nm, $\lambda 1$ is 500 nm, and $\lambda 2$ is 550 nm. Similar method is applied to model simulated AOD output to derive AOD at 550 nm.

Fig. 4 shows the spatial distributions of monthly mean MODIS-derived and model simulated AOD at 550 nm wavelength. With the largest amount of biogenic emissions occurring in the southeastern U.S. including Texas, an increase in AOD is simulated in this region when considering SOA in the model. Over the northeast part of the country, there is also an increase in AOD. The default model underestimates AOD over much of the abovementioned areas by 0.1−0.5, in particular, over the regions where the amount of biogenic emissions is significant. It should be noted that the model with or without SOA fails to capture the high AOD in the northwestern U.S.. This could be attributed to the lack of fire and dust emissions in the current simulations. Liao et al. (2007) also found a large underprediction in organic matter over this region, which they attributed to some uncounted primary emissions from some sources such as wildfires over the U.S. Since the current model does not include fire and dust emissions, the model calculated AOD values are subject to uncertainties from these sources.

The comparison of model results with ground-based measurements cannot be done with all available data, since the model grid represents the mean concentration of rather large areas. From this perspective, it is good to select the measurements that could represent different land surface features. Fig. 5 displays model simulated and AERONET measured daily mean AOD over three major sites (Fig. 5d), where the landscapes are different. Comparison at site HJAndrews and site BSRN_BAO_Boulder shows a better agreement except for two high peaks. The measured and simulated AOD values at the two locations are relatively low, and the contribution of biogenic SOA to the total aerosol is small. The two peaks of AOD observed in the measurements at the two sites are identified to be due to local fire events. High AOD values on July 2, 2002 at site BSRN_BAO_Boulder (Fig. 5b) are caused by a wildfire that occurred
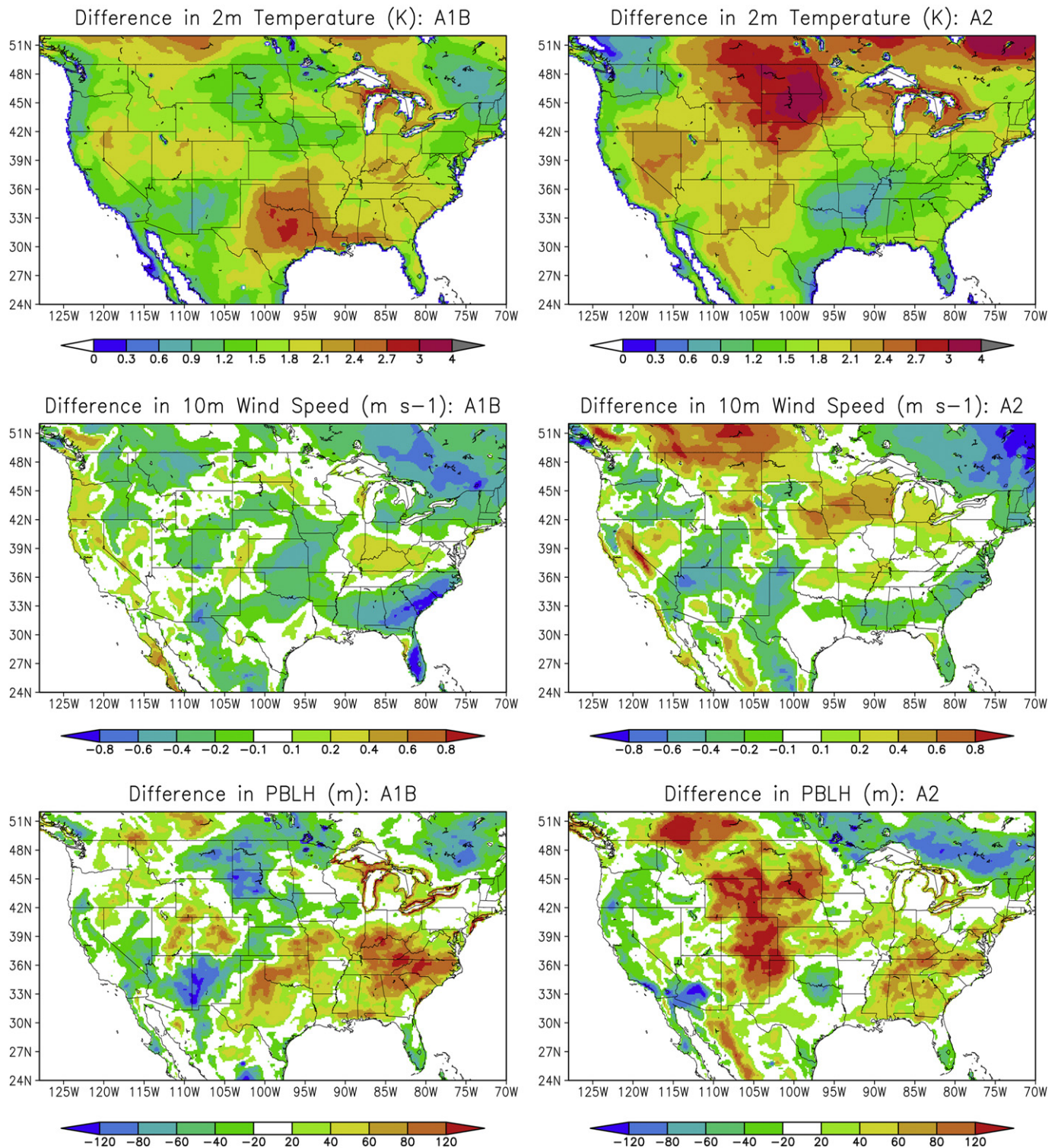
Fig. 7. Differences in temperature, wind speed, PBLH, cloud fraction (CLDFRA), precipitation and net shortwave radiation in July between 2050s (2051–2053) and 2000s (2001–2003) under the A1B and A2 scenarios.

between June 8 and July 2, 2002. It is also true for site HJAndrews (Fig. 5a), where high AOD values resulted from a nearby fire event, which occurred on July 21, 2002 in the Sierra Nevada Mountains of California. Again, this is due to the lack of fire emissions in the model. It is recommended to include them in future studies. Prediction at site Stennis (Fig. 5c) is quite promising, the simulated

AOD values with SOA model included agree well with measurements. The results suggest that considering SOA in the current model is important for aerosol prediction.

Fig. 6a compares simulated spatial distribution of monthly mean surface layer organic carbon (OC) concentrations in the presence of SOA with observations obtained from the IMPROVE network.
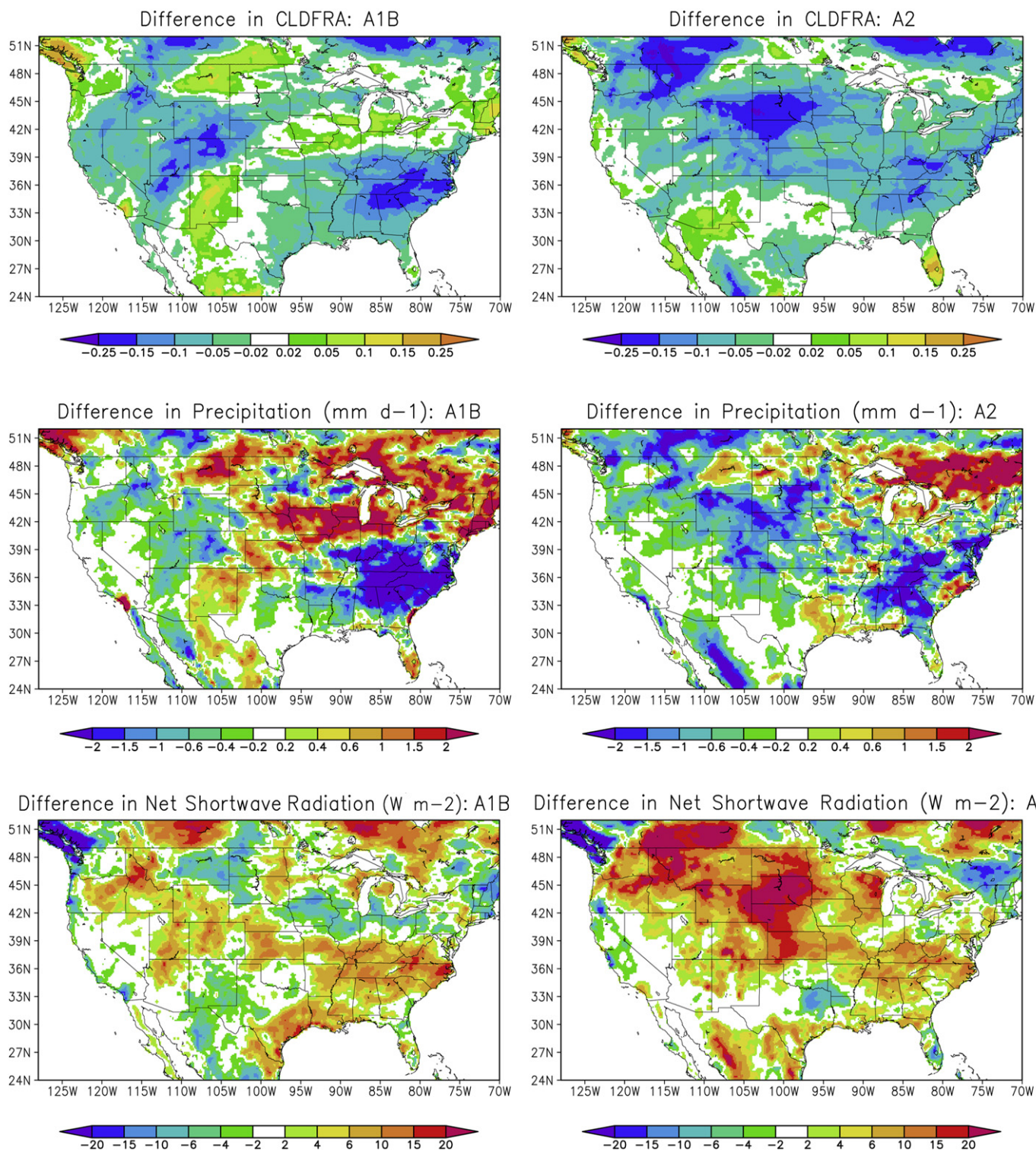
Fig. 7. (*continued*).

Overall, the model reasonably replicates the observed spatial distribution of OC over the U.S., with higher concentrations over the southeast and northwest regions. The simulated OC concentrations over the southeastern and northwestern U.S. are very close to the IMPROVE measurements. Some exceptions do exist. For instance, over some sites in the eastern U.S., observed OC concentrations are higher than the model simulated. The high concentrations of OC in

this region are mainly due to forest fires that occurred in Quebec, Canada during early July, 2002 (DeBell et al., 2004). A few high spots in the western U.S. are also due to the fire events. Over the Rocky mountain region, model underestimates OC. This, again, suggests the importance of including fire and dust emissions in the model. Fig. 6b and c mainly depict the primary organic carbon (POC) aerosols and the ratio of SOA in the total OC. The amount of

Table 3
Parameters used in the SOA model.

Hydrocarbon class	$O_3 + OH$ oxidation		NO_3 oxidation	$O_3 + OH$ oxidation		NO_3 oxidation
	α_1	α_2	α_3	K_1	K_2	K_3
I	0.0670	0.35425	1.0	0.1835	0.004275	0.0163
II	0.2390	0.3630	1.0	0.0550	0.0053	0.0163
III	0.06850	0.2005	1.0	0.1330	0.0035	0.0163
IV	0.06675	0.135	1.0	0.223750	0.0082	0.0163
V[a]	0.232	0.288	N/A	0.00862	1.62	N/A

α_i: stoichiometric coefficients; K_i: equilibrium gas-particle partition coefficients of semi-volatile compounds ($m^3\ \mu g^{-1}$) a: Only considered the reaction with OH.

SOA in OC is significant, with the ratio ranging from 0.1 to 0.5/0.6. This range agrees well with previous studies (Tsigaridis et al., 2005; Liao et al., 2007). Overall, comparisons between the simulated aerosol products and measurements suggest that the model has a relatively good performance in terms of simulating SOA over the U.S. The evaluation of the model performance gives us confidence to examine the future climate effects.

5. Projected future changes

This section presents changes in regional climate, biogenic emissions and aerosols concentrations due to future climate change. The success of the WRF/Chem model simulations using CCSM model output has been evaluated in Jiang et al. (2008). Their results show that the WRF/Chem model when forced with the CCSM model output is able to simulate meteorological conditions reasonably well. Therefore, the following description mainly focuses on projected changes.

5.1. Projected changes in regional climate

Climatic conditions not only affect the formation of SOA in a direct way through changing temperature, relative humidity, clouds, winds, PBLH, precipitation and radiation, but also influence SOA levels by changing biogenic emissions in an indirect way. The calculation of biogenic emissions took into account the effects of temperature and radiation under different climates. Differences between the present-year simulations and future-year simulations are calculated to estimate the projected regional climate change over the next 50 years.

Projected changes in regional climate are to some extent dependent on the projected global climate change which is also scenario-dependent. Fig. 7 shows the simulated changes in 2 m
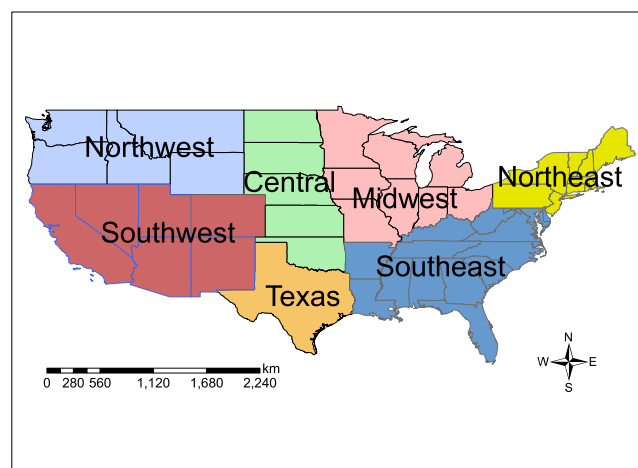

Fig. 8. Seven sub-regions in the United States (U.S.).

temperature, wind speed, PBLH, and cloud fraction based on the present-year and future-year simulations. In response to increased greenhouse gases in 2050s, the simulated surface warming under the A1B scenario occurs everywhere in the contiguous U.S., with the largest warming (>2 K) found over the Great Lakes region, the northwestern U.S., and Texas. The overall pattern of 2 m temperature change is identical with that presented in Zhang et al. (2008) in which they used a regional climate model to downscale global climate model output, but the regional details are slightly different. Areas with more warming tend to have reduced near-surface wind speed, enhanced PBLH, reduced cloud fraction, slightly reduced precipitation and increased shortwave radiation at the surface. Over the central Great Plains, the warming is much less as compared to the abovementioned regions. This small warming is also associated with decreased PBLH, increased cloud fraction, increased precipitation and slightly reduced shortwave radiation. Changes in these climate variables are intimately related.

In comparison with the A1B scenario, under the A2 emissions scenario, areas over the northern U.S. are expected to experience more warming, while the southern U.S. shows a relatively smaller warming. This is consistent with what presented in the IPCC report that if more greenhouse gases are put into the atmosphere, the mid-latitude and high-latitude regions would suffer more warming (IPCC, 2007). The changes in wind speed are also different from those observed under the A1B scenario. Over those areas with more warming, we see a slightly increase in wind speed. For the PBLH,

Table 4
Regional climate changes in seven sub-regions as shown in Fig. 8.

|	Southwest	Northwest	Texas	Central	Midwest	Southeast	Northeast
A1B							
2 m Temperature (K)	1.52	1.56	2.13	1.65	1.74	1.86	1.24
10 m Wind Speed (%)	0.03	−3.96	−0.03	−4.28	−1.34	−8.72	−14.37
Planetary Boundary Layer Height (%)	−0.02	−0.04	0.04	−1.72	3.89	7.87	0.67
Cloud Fraction (%)	−18.69	−12.18	−0.11	−8.47	−4.41	−34.82	4.84
Precipitation (%)	−4.82	−9.35	0.88	15.09	17.60	−26.30	32.61
Net Shortwave Radiation at the Surface (%)	0.19	0.36	0.01	0.32	0.01	2.04	−1.90
A2							
2 m Temperature (K)	1.92	1.82	1.61	2.28	1.93	1.22	1.65
10 m Wind Speed (%)	0.23	17.44	−0.05	27.58	28.64	−5.96	−12.30
Planetary Boundary Layer Height (%)	1.03	3.00	0.01	6.53	3.13	4.99	−0.94
Cloud Fraction (%)	−8.55	−28.39	−0.02	−30.58	−18.95	−21.76	−15.85
Precipitation (%)	0.76	−39.22	0.43	−22.72	−2.67	−8.67	0.62
Net Shortwave Radiation at the Surface (%)	0.01	3.45	0.00	4.64	1.65	1.40	−0.41
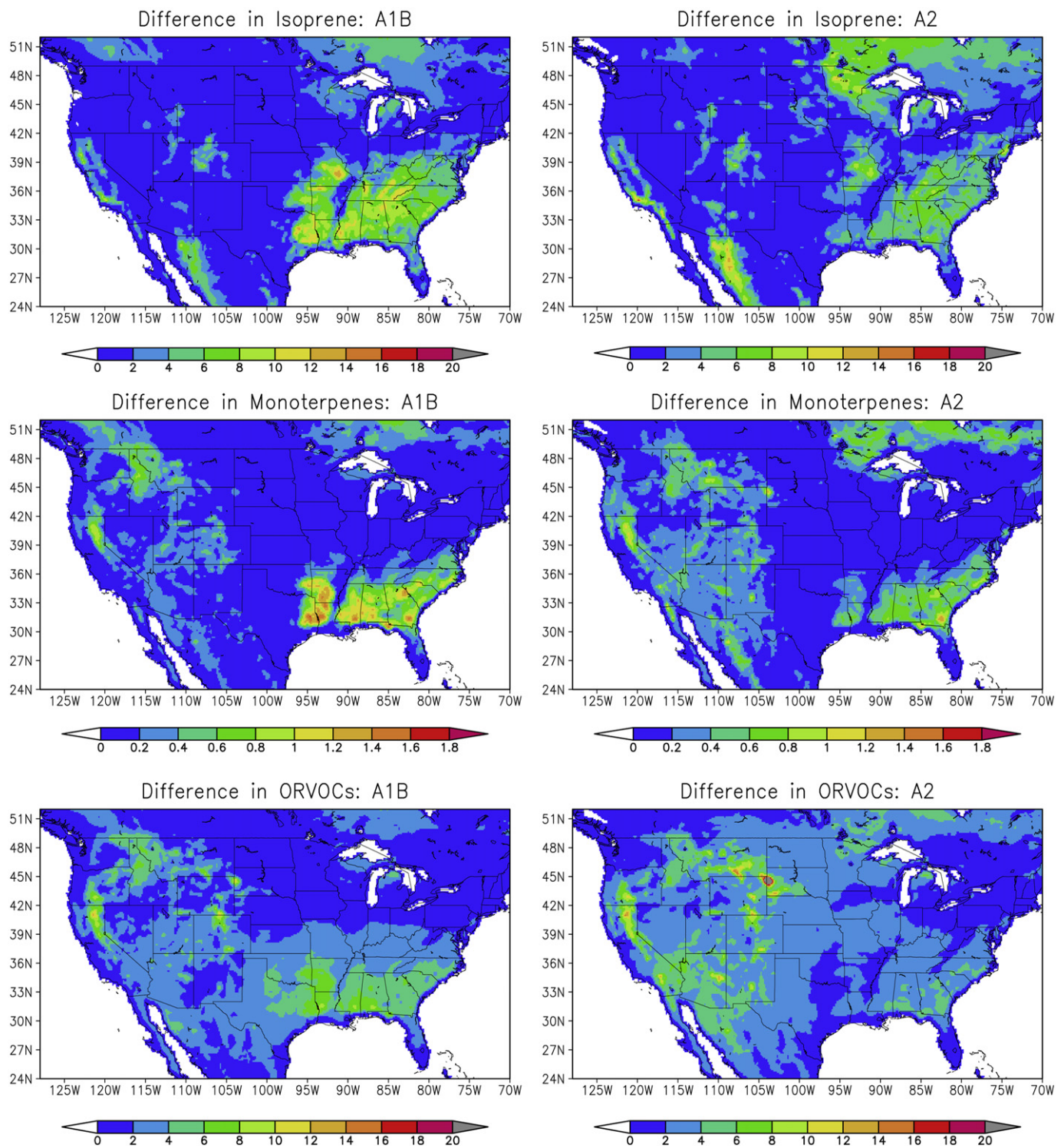
Fig. 9. As in Fig. 7, but for isoprene, monoterpenes, ORVOCs, and total biogenic emissions (mol km^{-2} h^{-1}).

the areas with more warming would still have higher PBLH. Cloud fraction always decreases under future warming climate. Warming is also associated with relatively increased shortwave radiation at the surface. Precipitation decreases over much of the modeling domain in response to future more warming. Comparing the two climate scenarios, differences are most pronounced in temperature, wind speed, PBLH, precipitation and shortwave radiation at the surface.

Quantitative changes in these climate variables under the two emissions scenarios (Table 4) are calculated over seven sub-regions (Fig. 8) in the U.S. On average, the largest temperature increases are projected to occur in Texas where Pye et al. (2009) also found the largest temperature increase in summer, while the smallest increases in temperature occur in the northwest under the A1B scenario. Under the A2 scenario, the largest increases in temperature (>2 K) are found over the central U.S., and the smallest
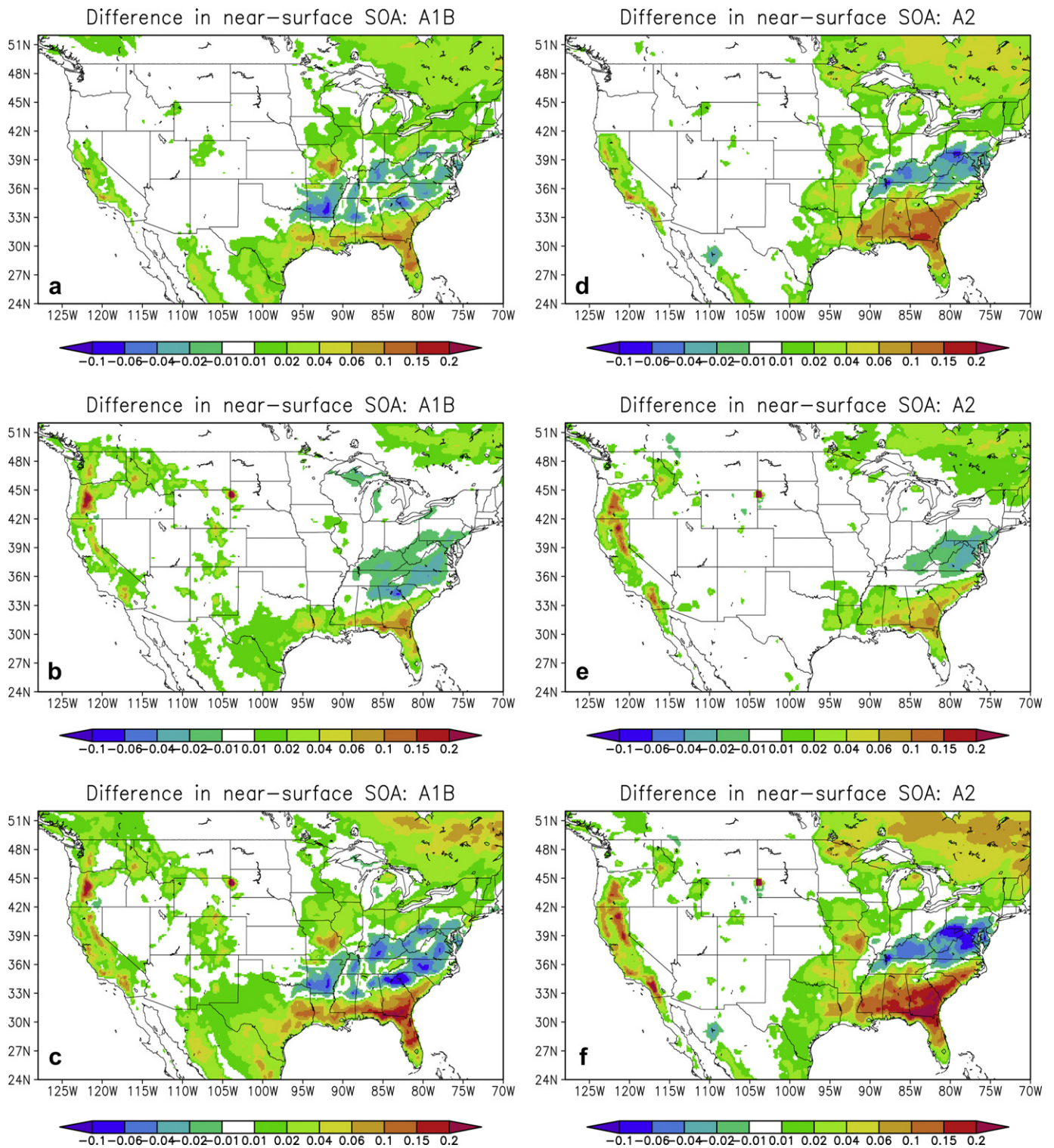
Fig. 10. As in Fig. 7, but for SOA concentrations (μg m^{-3}). (a) and (d) are the contribution from isoprene, (b) and (e) are the contribution from monoterpenes, and (c) and (f) are the total concentrations.

increase occurs over the southeastern U.S. An increase of 1.5−1.9 K in temperature is seen in the other regions. Changes in near-surface wind speed are more pronounced in the northwest, central, southeast and northeast, with the northeast experiencing the largest decrease under the A1B scenario. Under the A2 scenario, the regions which would experience more warming are projected to have strong near-surface wind. Over the eastern U.S. including the

northeast and southeast, the near-surface wind speed is expected to decrease due to relatively small increase in temperature. Changes in PBLH are more identical to changes in temperature. However, percentage of changes in PBLH is not as significant as that of wind speeds. Changes in cloud fraction are highly related to temperature changes under the two scenarios. Over the regions where the temperature changes are the largest, there are decreases
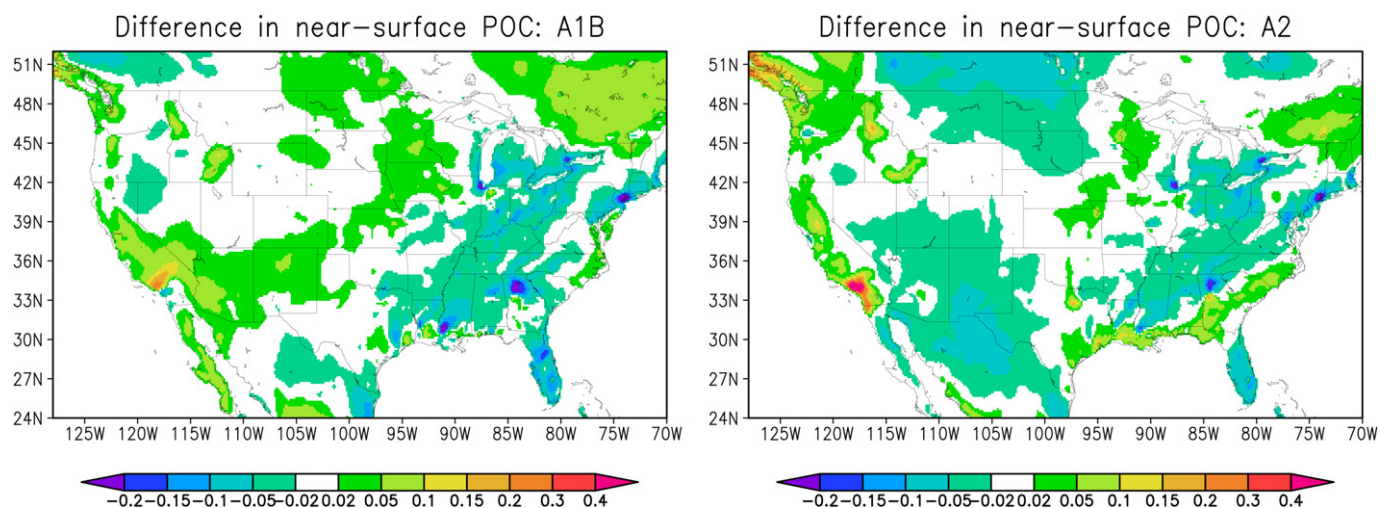
Fig. 11. As in Fig. 7, but for POC ($\mu g\ m^{-3}$).

5.2. Projected changes in biogenic emissions and SOA

in cloud fraction correspondingly, such as the southeast region (-34.8%) under the A1B scenario, and the northwest (-28.4%) and the central region (-30.6%) under the A2 scenario. As presented in the IPCC (2007) report, on average, the regions with the largest temperature increases tend to have less cloud coverage, thus a decrease in precipitation. As seen from the table, over the areas where we see more warming, there are significant decreases in precipitation, such as the southeast under the A1B scenario, the northwest and the central under the A2 scenario.

Overall, under the two climate scenarios, the projected warming and the related climate change, in particular winds and precipitation are variable everywhere. There are significant differences in regional details. Thus, we would expect these differences would attribute to differences in projected biogenic emissions, aerosols and SOA.

Changes in climate, especially temperature changes could affect biogenic emissions (e.g., Wiedinmyer et al., 2006). Fig. 9 shows predicted changes in monthly mean isoprene, monoterpenes, ORVOCs, and total biogenic emissions at the surface. Changes in projected biogenic emissions are different under different climate scenarios, in particular, over the southeast and west regions. As the algorithm used to calculate biogenic emissions is temperature and radiation-dependent, the spatial patterns of changes in biogenic emissions are strongly influenced by these variables. On average, projected temperature changes have the largest impact on biogenic emissions over the southeast region and the western U.S. Under the A1B scenario, more isoprene and monoterpenes are seen over the southeast region, whereas the amounts of isoprene and
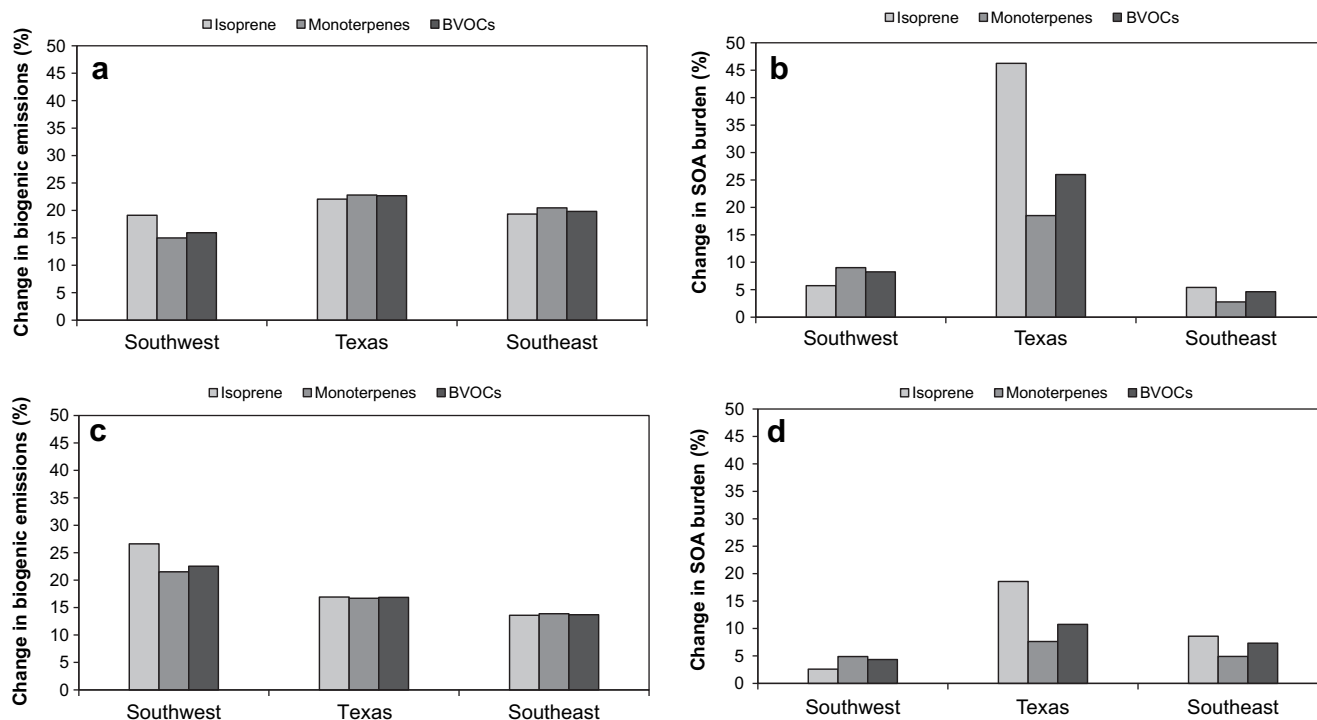

Fig. 12. Percentage changes of biogenic emissions and SOA concentrations in three regions (Southwest, Texas and Southeast) under the A1B and A2 scenarios.

monoterpenes are slightly less under the A2 scenario. This is mainly due to the temperature differences under the two scenarios as seen from Fig. 7a and b. In the northeastern U.S., more biogenic emissions are projected under the A2 scenario, as the temperature increase is larger than that under the A1B scenario.

Changes in climate and biogenic emissions can further influence aerosol burdens. Generally, warmer climate can influence aerosol burdens by changing aerosol wet deposition, altering climate-sensitive emissions, and shifting aerosol thermodynamic equilibrium. Fig. 10 shows the projected changes in SOA under the two climate scenarios. The overall changes in the spatial patterns are not identical with those of biogenic emissions or temperature. Although biogenic emissions increase under the future warmer climate, changes in SOA as a result of climate change are various over the domain. As noted above, an increase in biogenic emissions is found over the southeast region, while over this area, we see a decrease and an increase in SOA. This can be explained that not only the amount of biogenic emissions could affect SOA formation, but also climate variables such as temperature, wind and precipitation may play an important role in SOA formation and deposition. For example, since the model considers the effect of temperature on partitioning coefficients, the reduction in partitioning coefficients due to temperature increase in the future could lead to lower SOA concentrations near the surface. In addition to the effect of temperature on the partitioning coefficients, temperature increase could also affect the reaction rates of the gas-phase chemistry. Tsigaridis and Kanakidou (2007) studied the sensitivity of temperature on SOA formation, and they found lower SOA concentrations due to the effects on the partitioning coefficients and reaction rates of the gas-phase chemistry over some regions. Recent studies (Goldstein et al., 2009; Carlton et al., 2010) found that biogenic SOA can be strongly affected by anthropogenic emissions. This can also explain why the future changes in SOA are not identical with those in biogenic emissions.

The pre-existing POC aerosols could also play an important role in the SOA formation. The effects of future climate change on POC aerosols are shown in Fig. 11. Decreases in POC concentrations are found over the regions (e.g., the southeastern U.S.) where we see a decrease in SOA. This could be another factor driving the reduction in SOA in the future. Comparing the changes in SOA under the A1B and A2 scenarios, although more warming is seen under the A1B scenario over the southeastern U.S., the increase in SOA over this region is smaller than that under the A2 scenario. The non-linearity in SOA formation and the involved chemical and physical feedbacks make it different to quantitatively address the contributions of changes in SOA due to different factors. A more comprehensive study considering the effects of different factors might be helpful in understanding SOA formation under the different climate conditions, which is beyond the scope of the current study.

Results for percentage changes in biogenic emissions and SOA are only listed for the three regions—Southwest, Texas, and Southeast—because these regions are experiencing pronounced changes. Fig. 12 shows, on average, changes in biogenic emissions including isoprene and monoterpenes over the three regions are quite similar (around 20%), with Texas being the one having the largest increase in biogenic emissions under the A1B scenario in the future. If the climate scenario is A2, the biggest increase in biogenic emissions is seen over the southwest region (22%). Differences in biogenic emissions under the two different emissions scenarios can be explained by the differences in temperature increase in the future. Again, changes in SOA concentrations due to future climate change are not consistent with those of biogenic emissions. Under the A1B scenario, the biggest increase in SOA is found over Texas, with isoprene emissions being the major contributor to SOA

formation. The range of change varies from 5% over the southeast to 26% over Texas. As an alternative, our results about SOA changes in response to another climate scenario A2 show that SOA concentrations do not increase linearly with temperature increase. Using a global model, Heald et al. (2008) estimated a 26% increase due to the increase in biogenic emissions, a 6% increase due to the climate change, and a 35% increase due to the combined effect in 2010. On regional scales, Zhang et al. (2008) estimated an 18% decrease in predicted SOA concentrations due to the regional climate change by 2050s. These results suggest that there are uncertainties associated with different models. Future studies about the sensitivity of SOA to different factors are needed for a better understanding of effects of climate change and biogenic emissions on SOA.

6. Conclusions

A regional coupled land−atmosphere−chemistry model has been extended to include SOA formation. As there is no direct measurement of SOA on a large scale, the model performance is evaluated with available ground-based and satellite aerosol measurements including AOD and OC concentrations. The overall simulated spatial pattern of SOA agrees well with previous studies. The contribution of SOA to AOD is more pronounced over the area where there is a significant amount of biogenic emissions. The comparison also reveals that the model with the lack of aerosol sources from fire events and dusts underestimates AOD and OC over some regions, in particular in the northwestern U.S. Future studies with the model including fire and dust emissions are required to improve the model performance in terms of simulating aerosol concentrations.

The sensitivity of SOA to different climate scenarios is investigated with the model driven by global climate model output. Under the future A1B and A2 emissions scenarios, future temperature changes were predicted to increase everywhere in the U.S., but with different degrees of increase in different regions. More specifically, the largest temperature increases are projected to occur in Texas, while the smallest increases in temperature occur in the northwest under the A1B scenario. Under the A2 scenario, we found that the largest increases in temperature (>2 K) over the central U.S. and the smallest increases over the southeastern U.S. Over other regions, the temperature increase is around 1.5−1.9 K. Clearly, different climate scenarios lead to different temperature responses. These changes in temperature are also associated with changes in other climate variables such as wind speed, PBLH, precipitation and cloud fraction. As a result of climate change or temperature increase in the future, biogenic emissions are predicted to increase everywhere, with the largest increase found in the southeastern U.S. and the northwestern U.S. The increases under the two different climate scenarios are different due to the differences in temperature increases. Changes in SOA are not identical with those in biogenic emissions. Other factors such as partitioning coefficients, atmospheric oxidative capability, POC and anthropogenic emissions also play a role in SOA formation. Direct and indirect impacts from climate change complicate the future SOA formation. In order to gain a more accurate understanding of how future climate will affect SOA, more detailed sensitivity analysis of SOA formation is required.

Center for computing resources. We acknowledge the AERONET, MODIS and IMPROVE teams for use of their data.

References

Andersson-Skold, Y., Simpson, D., 2001. Secondary organic aerosol formation in northern Europe: a model study. Journal of Geophysical Research 106 (D7), 7357–7374.

Avise, J., Chen, J., Lamb, B., Wiedinmyer, C., Guenther, A.B., Salathe, E., Mass, C., 2009. Attribution of projected changes in summertime US ozone and PM2.5 concentrations to global changes. Atmospheric Chemistry and Physics 9, 1111–1124.

Axson, J.L., Takahashi, K., DeHaan, D., Vaida, V., 2010. Gas-phase water-mediated equilibrium between methylglyoxal and its geminal diol. Proceedings of the National Academy of Sciences, U.S.A 107 (15), 6687–6692.

Barnard, J.C., Chapman, E.G., Fast, J.D., Schmelzer, J.R., Slusser, J.R., Shetter, R.E., 2004. An evaluation of the FAST-J photolysis algorithm for predicting nitrogen dioxide photolysis rates under clear and cloudy sky conditions. Atmospheric Environment 38, 3393–3403.

Barth, M., McFadden, J., Sun, J., et al., 2005. Coupling between land ecosystems and the atmospheric hydrologic cycle through biogenic aerosol pathways. Bulletin of the American Meteorological Society 86, 1738–1742.

Baum, E.J., 1998. Chemical Property Estimation; Theory and Application. CRC Press LLC, Florida.

Binkowski, F.S., Shankar, U., 1995. The regional particulate matter model: 1. Model description and preliminary results. Journal of Geophysical Research 100, 26 191–26 209.

Calvert, J.G., Atkinson, R., Kerr, J.A., Madronich, S., Moortgat, G.K., Wallington, T.J., Yarwood, G., 2000. The Mechanisms of the Atmospheric Oxidation of the Alkenes. Oxford University Press, Oxford, pp. 552.

Carlton, A.G., Turpin, B.J., Lim, H.-J., Altieri, K.E., Seitzinger, S., 2006. Link between isoprene and secondary organic aerosol (SOA): pyruvic acid oxidation yields low volatility organic acids in clouds. Geophysical Research Letter 33, L06822. doi:10.1029/2005GL025374.

Carlton, A.G., Wiedinmyer, C., Kroll, J.H., 2009. A review of Secondary Organic Aerosol (SOA) formation from isoprene. Atmospheric Chemistry and Physics 9, 4987–5005.

Carlton, A.G., Pinder, R.W., Bhave, P.V., Pouliot, G.A., 2010. To what extent can biogenic SOA be controlled? Environmental Science & Technology 44, 3376–3380.

Chin, M., Rood, R.B., Lin, S.-J., Müller, J.-F., Thompson, A.M., 2000. Atmospheric sulfur cycle simulated in the global model GOCART: model description and global properties. Journal of Geophysical Research 105 (D20), 24,671–24,687.

Chung, S.H., Seinfeld, J.H., 2002. Global distribution and climate forcing of carbonaceous aerosols. Journal of Geophysical Research 107 (D19), 4407. doi:10.1029/2001JD001397.

Claeys, M., Graham, B., Vas, G., Wang, W., Vermeylen, R., Pashynska, V., Cafmeyer, J., Guyon, P., Andreae, M.O., Artaxo, P., Maenhaut, W., 2004. Formation of secondary organic aerosols through photooxidation of isoprene. Science 303, 1173–1176.

Collins, W.D., et al., 2006. Radiative forcing by well-mixed greenhouse gases: estimates from climate models in the Intergovernmental Panel on Climate Change (IPCC) Fourth Assessment Report (AR4). Journal of Geophysical Research 111, D14317. doi:10.1029/2005JD006713.

DeBell, L.J., Talbot, R.W., Dibb, J.E., Munger, J.W., Fischer, E.W., Frolking, S.E., 2004. A major regional air pollution event in the northeastern United States caused by extensive forest fires in Quebec, Canada. Journal of Geophysical Research 109, D19305. doi:10.1029/2004JD004840.

Donahue, N., Robinson, A., Stanier, C., Pandis, S., 2006. Coupled partitioning, dilution, and chemical aging of semivolatile organics. Environmental Science & Technology 40 (8), 2635–2643. doi:10.1021/es052297c.

Donahue, N.M., Robinson, A.L., Pandis, S.N., 2009. Atmospheric organic particulate matter: from smoke to secondary organic aerosol. Atmospheric Environment 43 (1), 94e106. doi:10.1016/j.atmosenv.2008.09.055.

Dudhia, J., 1989. Numerical study of convection observed during the winter monsoon experiment using a mesoscale two-dimensional model. Journal of the Atmospheric Sciences 46, 3077–3107.

El Haddad, I., Liu, Y., Nieto-Gligorovski, L., Michaud, V., Temime-Roussel, B., Quivet, E., Marchand, N., Sellegri, K., Monod, A., 2009. In-cloud processes of methacrolein under simulated conditions – part 2: formation of secondary organic aerosol. Atmospheric Chemistry and Physics 9, 5107–5117.

Farina, S.C., Adams, P.J., Pandis, S.N., 2010. Modeling global secondary organic aerosol formation and processing with the volatility basis set: implications for anthropogenic secondary organic aerosol. Journal of Geophysical Research 115, D09202. doi:10.1029/2009JD013046.

Fast, J.D., Gustafson Jr., W.I., Easter, R.C., Zaveri, R.A., Barnard, J.C., Chapman, E.G., Grell, G.A., Peckham, S.E., 2006. Evolution of ozone, particulates, and aerosol direct radiative forcing in the vicinity of Houston using a fully coupled meteorology–chemistry–aerosol model. Journal of Geophysical Research 111, D21305. doi:10.1029/2005JD006721.

Goldstein, A.H., Koven, C.D., Heald, C.L., Fung, I.Y., 2009. Biogenic carbon and anthropogenic pollutants combine to form a cooling haze over the southeastern United States. Proceedings of the National Academy of Sciences 106, 8835–8840. doi:10.1073/pnas.0904128106.

Grell, G.A., Peckham, S.E., Schmitzc, R., McKeenb, S.A., Frostb, G., Skamarockd, W.C., Eder, B., 2005. Fully coupled "online" chemistry within the WRF model. Atmospheric Environment 39, 6957–6975.

Griffin, R.J., Cocker III, D.R., Seinfeld, J.H., Dabdub, D., 1999. Estimate of global atmospheric organic aerosol from oxidation of biogenic hydrocarbons. Geophysical Research Letters 26 (17), 2721–2724.

Griffin, R.J., Dabdub, D., Kleeman, M.J., Fraser, M.P., Cass, G.R., Seinfeld, J.H., 2002. Secondary organic aerosol: III. Urban/Regional scale model of size- and composition-resolved aerosols. Journal of Geophysical Research 107 (D17), 4334. doi:10.1029/2001JD000544.

Guenther, A., et al., 1995. A global model of natural volatile organic compound emissions. Journal of Geophysical Research 100 (D5), 8873–8892. doi:10.1029/94JD02950.

Heald, C.L., et al., 2008. Predicted change in global secondary organic aerosol concentrations in response to future climate, emissions, and land use change. Journal of Geophysical Research 113, D05211. doi:10.1029/2007JD009092.

Henze, D.K., Seinfeld, J.H., 2006. Global secondary organic aerosol from isoprene oxidation. Geophysical Research Letters 33, L09812. doi:10.1029/2006GL025976.

Hogrefe, C., Lynn, B., Civerolo, K., Ku, J.-Y., Rosenthal, J., Rosenzweig, C., Goldberg, R., Gaffin, S., Knowlton, K., Kinney, P.L., 2004. Simulating changes in regional air pollution over the eastern United States due to changes in global and regional climate and emissions. Journal of Geophysical Research 109, D22301. doi:10.1029/2004JD004690.

Hong, S.Y., Pan, H.L., 1996. Nonlocal boundary layer vertical diffusion in a medium-range forecast model. Monthly Weather Review 124, 2322–2339.

Hoyle, C.R., Myhre, G., Berntsen, T.K., Isaksen, I.S.A., 2009. Anthropogenic influence on SOA and the resulting radiative forcing. Atmospheric Chemistry and Physics 9, 2715–2728.

Intergovernmental Panel on Climate (IPCC)Change, 2007. In: Solomon, S., et al. (Eds.), Climate Change 2007: The Scientific Basis. Contribution of Working Group I to the Fourth Assessment Report of the Intergovernmental Panel on Climate Change. Cambridge Univ. Press, New York.

Jacob, D.J., Winner, D.A., 2009. Effect of climate change on air quality. Atmospheric Environment 43, 51–63.

Jiang, X., Wiedinmyer, C., Chen, F., Yang, Z.-L., Lo, J.C.-F., 2008. Predicted impacts of climate and land use change on surface ozone in the Houston, Texas, area. Journal of Geophysical Research 113, D20312. doi:10.1029/2008JD009820.

Jimenez, J.L., et al., 2009. Evolution of organic aerosols in the atmosphere. Science 326, 1525–1529. doi:10.1126/science.1180353.

Kain, J.S., Fritsch, M., 1990. A one-dimensional entraining/detraining plume model and its application in convective parameterization. Journal of the Atmospheric Sciences 47, 2784–2802.

Kanakidou, M., et al., 2005. Organic aerosol and global climate modelling: a review. Atmospheric Chemistry and Physics 5, 1053–1123.

Karl, M., Tsigaridis, K., Vignati, E., Dentener, F., 2009. Formation of secondary organic aerosol from isoprene oxidation over Europe. Atmospheric Chemistry and Physics 9, 7003–7030. doi:10.5194/acp-9-7003-2009.

Kesselmeier, J., Staudt, M., 1999. Biogenic Volatile Organic Compounds (VOC): an overview on emission, physiology and ecology. Journal of Atmospheric Chemistry 33, 23–28.

Kinnee, E., Geron, C., Pierce, T., 1997. United States land use inventory for estimation biogenic ozone precursor emissions. Ecological Applications 7, 46–58.

Kroll, J.H., Seinfeld, J.H., 2008. Chemistry of secondary organic aerosol: formation and evolution of low-volatility organics in the atmosphere. Atmospheric Environment 42, 3593–3624.

Kroll, J.H., Ng, N.L., Murphy, S.M., Flagan, R.C., Seinfeld, J.H., 2006. Secondary organic aerosol formation from isoprene photooxidation. Environmental Science & Technology 40, 1869–1877. doi:10.1021/es0524301.

Lack, D.A., Tie, X.X., Bofinger, N.D., Wiegand, A.N., Madronich, S., 2004. Seasonal variability of secondary organic aerosol: a global modelling study. Journal of Geophysical Research 109, D03203. doi:10.1029/2003JD003418.

Levis, S., Wiedinmyer, C., Bonan, G.B., Guenther, A.B., 2003. Simulating biogenic volatile organic compound emissions in the Community Climate System Model. Journal of Geophysical Research 108 (D21), 4659. doi:10.1029/2002JD003203.

Liao, H., Chen, W.-T., Seinfeld, J.H., 2006. Role of climate change in global predictions of future tropospheric ozone and aerosols. Journal of Geophysical Research 111, D12304. doi:10.1029/2005JD006852.

Liao, H., Henze, D.K., Seinfeld, J.H., Wu, S., Mickley, L.J., 2007. Biogenic secondary organic aerosol over the United States: comparison of climatological simulations with observations. Journal of Geophysical Research 112, D06201. doi:10.1029/2006JD007813.

Lide, D.R. (Ed.), 2001. CRC Handbook of Chemistry and Physics. CRC Press, Boca Raton, Fla.

Lin, Y.-L., Rarley, R.D., Orville, H.D., 1983. Bulk parameterization of the snow field in a cloud model. Journal of Applied Meteorology 22, 1065–1092.

Meehl, G.A., et al., 2006. Climate change projections for the twenty-first century and climate change commitment in the CCSM3. Journal of Climate 19 (11), 2597–2616.

Mesinger, F., Dimego, G., Kalnay, E., Mitchell, K., Sharfran, P.C., Ebisuzaki, W., Jovic, D., Rodgers, E., Berbery, E., Ek, M.B., Fan, Y., Grumbine, R., Higgins, W., Li, H., Lin, Y., Manikin, G., Parrish, D., Shi, W., 2006. North American regional reanalysis. Bulletin of the American Meteorological Society 87, 343–360.

Mlawer, E.J., Taubman, S.J., Brown, P.D., Iacono, M.J., Clough, S.A., 1997. Radiative transfer for inhomogeneous atmospheres: RRTM, a validated correlated-k model for the longwave. Journal of Geophysical Research 102 (D14), 16,663–16,682.

Nakicenovic, N., et al., 2000. IPCC Special Report on Emissions Scenarios. Cambridge University Press, Cambridge, United Kingdom and New York, NY, USA, 599 pp.

Ng, N.L., Kroll, J.H., Keywood, M.D., Bahreini, R., Varutbangkul, V., Flagan, R.C., Seinfeld, J.H., Lee, A., Goldstein, A.H., 2006. Contribution of first- versus second-generation products to secondary organic aerosols formed in the oxidation of biogenic hydrocarbons. Environmental Science & Technology 40 (7), 2283–2297. doi:10.1021/es052269u.

Odum, J.R., Jungkamp, T.P.W., Griffin, R.J., Forstner, H.J.L., Flagan, R.C., Seinfeld, J.H., 1997. Aromatics, reformulated gasoline, and atmospheric organic aerosol formation. Environmental Science and Technology 31 (7), 1890–1897.

Offenberg, J.H., Kleindienst, T.E., Jaoui, M., Lewandowski, M., Edney, E.O., 2006. Thermal properties of secondary organic aerosols. Geophysical Research Letter 33, L03816. doi:10.1029/2005GL024623.

Pankow, J.F., 1994. An absorption model of gas/particle partitioning involved in the formation of secondary organic aerosol. Atmospheric Environment 28, 189–193.

Pun, B., Seigneur, C., 2008. Organic aerosol spatial/temporal patterns: perspective of measurements and model. Environmental Science & Technology 42, 7287–7293.

Pye, H.O.T., Liao, H., Wu, S., Mickley, L.J., Jacob, D.J., Henze, D.K., Seinfeld, J.H., 2009. Effect of changes in climate and emissions on future sulfate–nitrate–ammonium aerosol levels in the United States. Journal of Geophysical Research 114, D01205. doi:10.1029/2008JD010701.

Robinson, A.L., Donahue, N.M., Shrivastava, M.K., et al., 2007. Rethinking organic aerosols: semivolatile emissions and photochemical aging. Science 315, 1259–1262.

Sakulyanontvittaya, T., Guenther, A., Helmig, D., Milford, J., Wiedinmyer, C., 2008. Secondary organic aerosol from sesquiterpene and monoterpene emissions in the United States. Environmental Science & Technology 42 (23), 8784–8790.

Seinfeld, J.H., Pankow, J.F., 2003. Organic atmospheric particulate material. Annual Review of Physical Chemistry 54, 121–140.

Skamarock, W.C., Klemp, J.B., Dudhia, J., Gill, D.O., Barker, D.M., Wang, W., Powers, J.D., 2005. A Description of the Advanced Research WRF Version 2.Technical Report. National Center for Atmospheric Research, TN-468+STR, 88 pp.

Smirnov, A., Holben, B.N., Eck, T.F., Dubovik, O., Slutsker, I., 2000. Cloud-screening and quality control algorithms for the AERONET database. Remote Sensing of Environment 73, 337–349.

Tagaris, E., Manomaiphiboon, K., Liao, K.-J., Leung, L.R., Woo, J.-H., He, S., Amar, P., Russell, A.G., 2007. Impacts of global climate change and emissions on regional ozone and fine particulate matter concentrations over the United States. Journal of Geophysical Research 112, D14312. doi:10.1029/2006JD008262.

Tsigaridis, K., Kanakidou, M., 2003. Global modelling of secondary organic aerosol in the troposphere: a sensitivity analysis. Atmospheric Chemistry and Phys 3, 1849–1869.

Tsigaridis, K., Kanakidou, M., 2007. Secondary organic aerosol importance in the future atmosphere. Atmospheric Environment 41, 4682–4692.

Tsigaridis, K., Lathiere, J., Kanakidou, M., Hauglustaine, D.A., 2005. Naturally driven variability in the global secondary organic aerosol over a decade. Atmos. Chem. Phys. Discuss. 5, 1255–1283.

Volkamer, R., Ziemann, P.J., Molina, M.J., 2009. Secondary Organic Aerosol Formation from acetylene (C_2H_2): seed effect on SOA yields due to organic photochemistry in the aerosol aqueous phase. Atmospheric Chemistry and Physics 9, 1907–1928.

Vukovich, J., Pierce, T., 2002. The implementation of BEIS3 within the SMOKE modeling framework. In: Proc. 11th International Emission Inventory Conference: Emission Inventories – Partnering for the Future, Atlanta, GA. US EPA CD-ROM, 10.7.

Wesley, M.L., 1989. Parameterization of surface resistance to gaseous dry deposition in regional numerical models. Atmospheric Environment 16, 1293–1304.

Wiedinmyer, C., Tie, X.X., Guenther, A., Neilson, R., Granier, C., 2006. Future changes in biogenic isoprene emissions: how might they affect regional and global atmospheric chemistry? Earth Interactions 10 (3), 1–19.

Wild, O., Zhu, X., Prather, M.J., 2000. Fast-J: accurate simulation of in- and below-cloud photolysis in tropospheric chemical models. Journal of Atmospheric Chemistry 37, 245–282.

Zaveri, R.A., Peters, L.K., 1999. A new lumped structure photochemical mechanism for large-scale applications. Journal of Geophysical Research 104, 30387–30415.

Zaveri, R.A., Easter, R.C., Fast, J.D., Peters, L.K., 2008. Model for simulating aerosol interactions and chemistry (MOSAIC). Journal of Geophysical Research 113, D13204. doi:10.1029/2007JD008782.

Zhang, Y., Huang, J.-P., Henze, D.K., Seinfeld, J.H., 2007. Role of isoprene in secondary organic aerosol formation on a regional scale. Journal of Geophysical Research 112, D20207. doi:10.1029/2007JD008675.

Zhang, Y., Hu, X.-M., Leung, L.R., Gustafson Jr., W.I., 2008. Impacts of regional climate change on biogenic emissions and air quality. Journal of Geophysical Research 113, D18310. doi:10.1029/2008JD009965.